Pergamon

0301-9322(95)00048-8

Int. J. Multiphase Flow Vol. 21, No. 6, pp. 1107–1121, 1995

0301-9322/95 $9.50 + 0.00

AIR ENTRAINMENT IN TWO-DIMENSIONAL TURBULENT SHEAR FLOWS WITH PARTIALLY DEVELOPED INFLOW CONDITIONS

H. CHANSON
Department of Civil Engineering, The University of Queensland, Brisbane QLD 4072, Australia

(Received 27 October 1994; in revised form 11 June 1995)

Abstract—In plunging jet flows and at hydraulic jumps, large quantities of air are entrained at the intersection of the impinging flow and the receiving body of water. The air bubbles are entrained into a turbulent shear layer and strong interactions take place between the air bubble advection/diffusion process and the momentum shear region. New air–water flow experiments were conducted with two free shear layer flows: a vertical supported jet and a horizontal hydraulic jump. The inflows were partially developed boundary layers, characterized by the presence of a velocity potential core next to the entrapment point. In both cases, the distributions of air concentration exhibit a Gaussian distribution profile with an exponential longitudinal decay of the maximum air content. Interestingly, the location of the maximum air content and the half-value band width are identical for both flow situations, i.e. independent of buoyancy effects.

Key Words: air entrainment, turbulent shear flow, hydraulic jump, plunging jet, partially developed inflow

1. INTRODUCTION

When a plunging water jet impacts the free-surface of a receiving pool of water, large quantities of air are entrained at the intersection of the jet with the pool [figure 1(A)]. Immediately downstream of the jet impact, a free shear layer develops and interacts with the diffusion of the entrained air bubbles. Several researchers investigated the air entrainment at plunging jets (e.g. Van De Sande & Smith 1973; Ervine *et al.* 1980) and recent reviews include Wood (1991) and Bin (1993). But only two studies (Van De Donk 1981; Bonetto & Lahey 1993) recorded the air concentration profiles in the developing flow region, and no analysis of the air bubble diffusion mechanisms within the free shear layers was reported.

A "limiting" case of the free shear layer is the hydraulic jump. In open channels, the transition from a rapid to tranquil flow is called a hydraulic jump. It is distinguished by the development of large-scale turbulence, energy dissipation and air entrainment [figure 1(B)]. The air is entrained at the jump toe into a free shear layer, characterized by intensive turbulence production, predominantly in vortices with axes perpendicular to the flow direction. For a hydraulic jump in a horizontal rectangular channel, three types of inflow conditions are distinguished: a partially developed supercritical flow, a fully developed boundary layer flow and a pre-entrained jump†. In the present study, a hydraulic jump with partially developed inflow conditions is considered because of its similarity with most smooth turbulent plunging jet situations.

In this paper, new experimental data of air bubble diffusion in turbulent shear flows are reported (table 1). Two flow situations were investigated: a vertical supported jet and a horizontal hydraulic jump. A vertical supported plunging jet is defined as a two-dimensional plunging jet bounded between a vertical support and a free-surface [figure 1(A)]. For inflow conditions with thin boundary layers, the support can be assimilated to the centreline of a free jet (by applying the theory of images); and the single shear layer is representative of one half of the developing flow region.

Firstly, the experimental facilities are presented. Then the structure of the air–water flows is described. Experimental data are later presented, and an analogy between the two flow situations

†When the upstream flow is aerated, the presence of air bubbles within the flow and near the free-surface modifies the jump behaviour and characteristics: such a jump is called a "pre-entrained" hydraulic jump.

(A) - Air bubble entrainment at a vertical supported jet

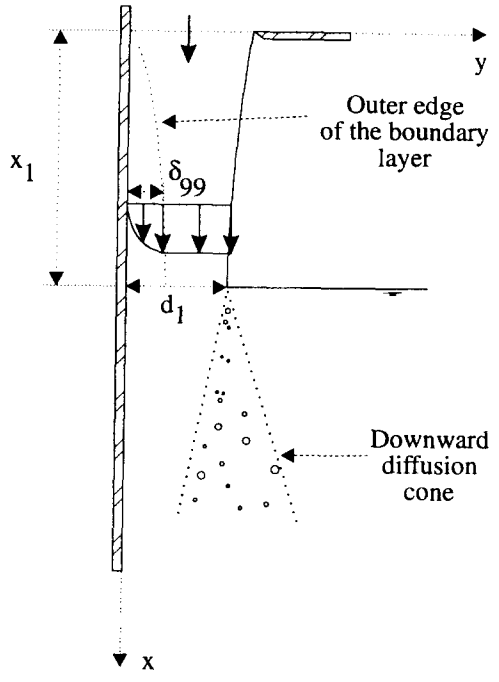

(B) Hydraulic jump with partially developed inflow conditions

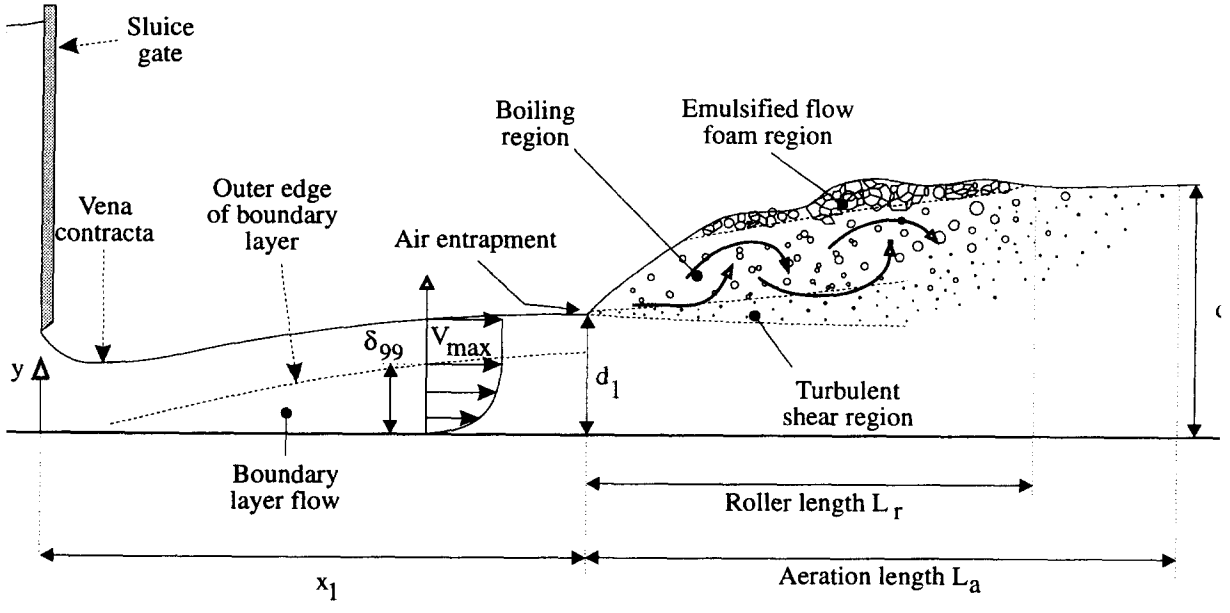

Figure 1. Air–water flow regions in turbulent shear layers.

Table 1. Experimental flow conditions of air–water flows

Ref. (1)	Run (2)	q_w (m²/s) (3)	V_1 (m/s) (4)	x_1 (m) (5)	Comments (6)
Vertical jets					
Present study	F1	0.024	2.36	0.090	Supported jet $W = 0.269$ m
	F2	0.048	4.06	0.090	
	F3	0.072	5.89	0.090	
	F4	0.096	8.0	0.090	
	F5	0.108	9.0	0.090	
Van De Donk (1981)					Circular jet
			4.463	0.20†	Fig. 3.22. $\phi_1 = 0.0057$ m
			10.19	0.20†	Fig. 3.23. $\phi_1 = 0.0059$ m
Bonetto & Lahey (1993)					Circular jet
	B11		6.18	0.03†	Fig. 11. $\phi_1 = 0.0051$ m
	B13		8.91	0.03†	Fig. 13. $\phi_1 = 0.0051$ m
Chanson & Cummings (1994a)			2.39	0.09	Supported jet
			6.14	0.09	$W = 0.269$ m
Hydraulic jumps					
Present study	C0	0.0504	3.190	0.963	$W = 0.25$ m
	C1	0.050	3.165	0.94	
	P10	0.0420	2.471	0.890	
	C2	0.0352	2.228	0.669	
	C3	0.0312	1.975	0.696	
Rajaratnam (1965)	A to I	0.073 to 0.144	1.95 to 3.99		Partially developed inflow $W = 0.308$ m
Resch & Leutheusser (1972)		0.0339	1.841		Partially developed inflow
		0.0718	2.779		$W = 0.39$ m
Thandaveswara (1974)	R1	0.0302	2.477		Normal hydraulic jump $W = 0.6096$ m
	R2	0.03484	2.656		
	R3	0.04184	3.907		
	R4	0.04887	4.216		
	R5	0.05612	4.598		
	R6	0.06086	4.007		
Ohtu *et al.* (1990)	Case a	0.04–0.06			Partially developed inflow [case (a)] $W = 0.15$ m. $0.014 < d_1 < 0.04$ m $2 < Fr_1 < 10$
	Case b	0.022–0.045			Fully-developed inflow [case (b)] $W = 0.4$ m. $0.011 < d_1 < 0.036$ m $2 < Fr_1 < 6$

†Distance between the nozzle and the free-surface pool.
W = channel width.
ϕ_1 = circular jet diameter at the impact with the free-surface pool.
Fr_1 = upstream Froude number: $Fr_1 = V_1/\sqrt{g*d_1}$.

is developed (figure 1). The results provide new information on the air distribution within the shear layers. The full set of data is reported in Chanson (1995).

2. EXPERIMENTAL APPARATUS

The experimental investigations were conducted in two separate flumes. The same instrumentation was used for each series of experiments, and domestic water was used in all experiments

The plunging jet experiments were performed using a two-dimensional vertical supported jet facility [figure 1(A)]. The apparatus consists of a glass tank with a depth of 1.8 m, a width of 0.30 m and a length of 3.6 m. A PVC rotatable slot nozzle supplies a planar supported jet, 0.27 m wide and 0.012 m thick. The length of the plate that supported the jet was 0.35 m and its inclination with the horizontal was 89° for all experiments. The water supply comes from a constant head tank which has a constant water level of 12.9 m above the nozzle.

The hydraulic jump experiments were conducted in a 3.20-m long channel of uniform rectangular section (width $W = 0.25$ m) [figure 1(B)]. Both walls and bed are made of glass (3.20-m long panels) and the channel is horizontal. Regulated flows are supplied through an adjustable vertical sluice gate. During the experiments, the gate opening was fixed at 20 mm. The experimentally-observed values for the coefficient of contraction (i.e. vena contracta) were equal to 0.6. These observations are very

close to the Von Mises (1971) solution for the no-gravity case. Tailwater levels were controlled by an overshoot sharp-crested gate at the downstream end of the channel.

The depth of the approach flows was measured using a pointer gauge positioned over the channel centreline. The approach flow velocity distributions were measured using a Pitot tube. The Pitot tube has an external diameter $\phi = 3.3$ mm, the total head being measured through a 1 mm hole at the tip, and the distance between the tip of the probe and the lateral pressure points ($\phi = 0.5$ mm) is 20 mm. During the experiments, the Pitot tube was connected either to a ValidyneTM DP15 pressure transducer scanned at 500 Hz or to a vertical manometer used to calibrate the transducer. Identical results were obtained with both systems.

(A) Run F1, $x_1 = 0.09$ m, $V_1 = 2.36$ m/s, $d_1 = 0.0102$ m

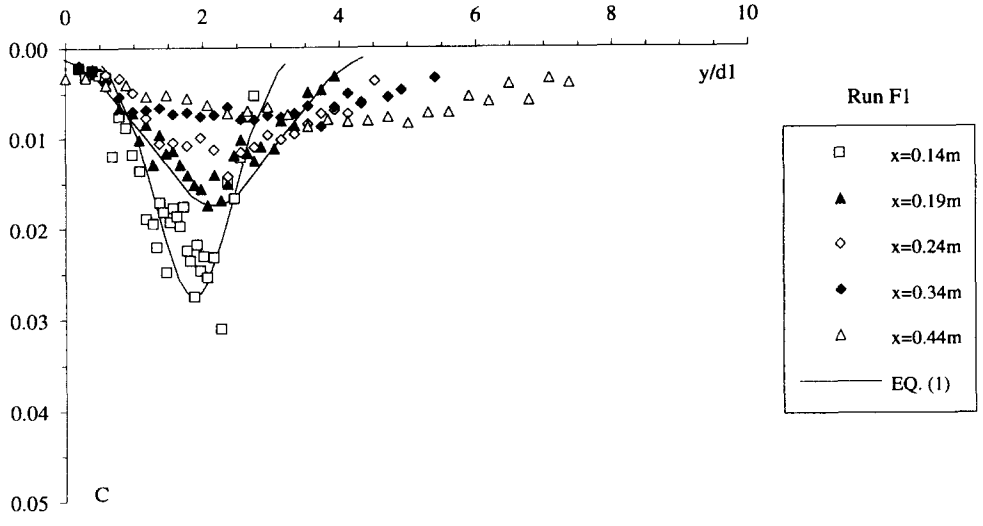

(B) Run F3, $x_1 = 0.09$ m, $V_1 = 5.89$ m/s, $d_1 = 0.0122$ m

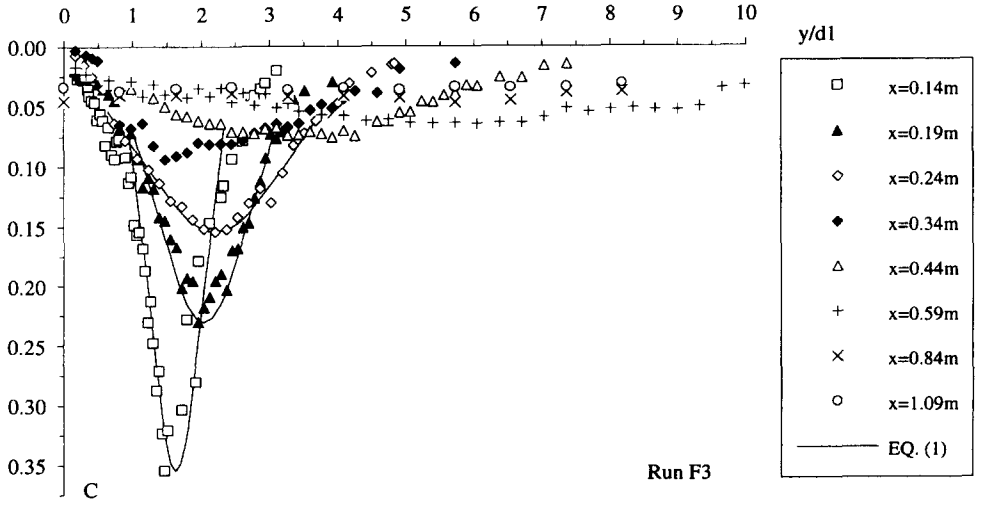

Figure 2(A) and (B). *Caption opposite*

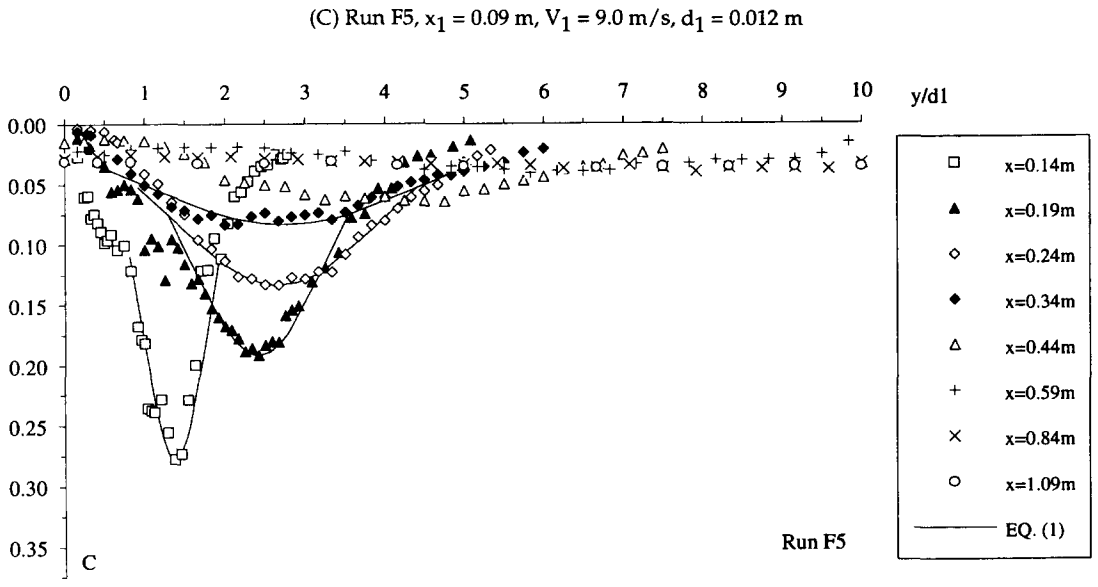

Figure 2(C)

Figure 2. Air concentration distributions at a vertical supported jet.

Air concentration measurements were performed with a single-tip conductivity probe similar to a previous design described in Chanson (1988, 1993, 1995). The probe consists of a sharpened rod (platinum wire $\phi = 0.35$ mm) which is insulated except for its tip and set into a metal supporting tube (stainless steel surgical needle $\phi = 1.42$ mm) acting as the second electrode. The conductivity probe was excited by an air bubble detector (AS25240) connected to a digital multimeter. The air bubble detector is an electronic circuit designed specifically to minimize the noise and the response time of the probe, cable and electronics. It was calibrated with a square wave generator and it was designed with a response time less than 10 μs.

Further, additional information was obtained by visual observations using high-speed photographs (flash speed of 33 μs) (see figure 4) and high-speed videocamera images (shutter speed of 500 μs).

2.1. Approach flow conditions

During the plunging jet experiments (table 1), the free-surface of the receiving pool of water was located 0.09 m below the jet nozzle. At the jet impact with the free-surface, the relative boundary layer thickness δ_{99}/d_1 was less than 0.2. For all the hydraulic jump experiments, the jump toe was located at $x_1 = 0.65$ to 0.96 m from the sluice gate. For such locations, the relative boundary layer thickness δ_{99}/d_1 was between 0.45 and 0.95 (Chanson & Qiao 1994).

3. EXPERIMENTAL RESULTS

3.1. Presentation

Air concentration distributions were measured below the entrainment point of the plunging jet and along the hydraulic jump. Typical profiles are plotted in figures 2 and 3.

At the supported plunging jet, the air concentration distributions are almost symmetrical, shifting slowly away from the support as the distance along the support increases. Note that the measurements obtained at $x > 0.35$ m were performed below the lower end of the support. As a result, the data might have been affected by the wake of the support. With circular jets, Van De Donk (1981) and Bonetto & Lahey (1993) observed air content profiles in the developing flow region with a shape similar to the results shown in figure 2.

With the hydraulic jump experiments, a major feature of the air concentration profiles is a region of high air content immediately downstream of the intersection of the upstream flow with the roller (figure 3). A large amount of air is entrained into this region of high shear stress, where the entrained air pockets are broken up into a large number of small-size bubbles. Other researchers observed a similar shape of the air concentration profiles in hydraulic jumps with partially developed upstream flows: e.g. Resch *et al.* (1972, 1974) and Thandaveswara (1974). Note that fully developed hydraulic jumps and pre-entrained hydraulic jumps exhibit different air concentration distributions, in particular without a high air content core.

(A) Run P10, x_1 = 0.890 m, V_1 = 2.47 m/s, d_1 = 0.017 m

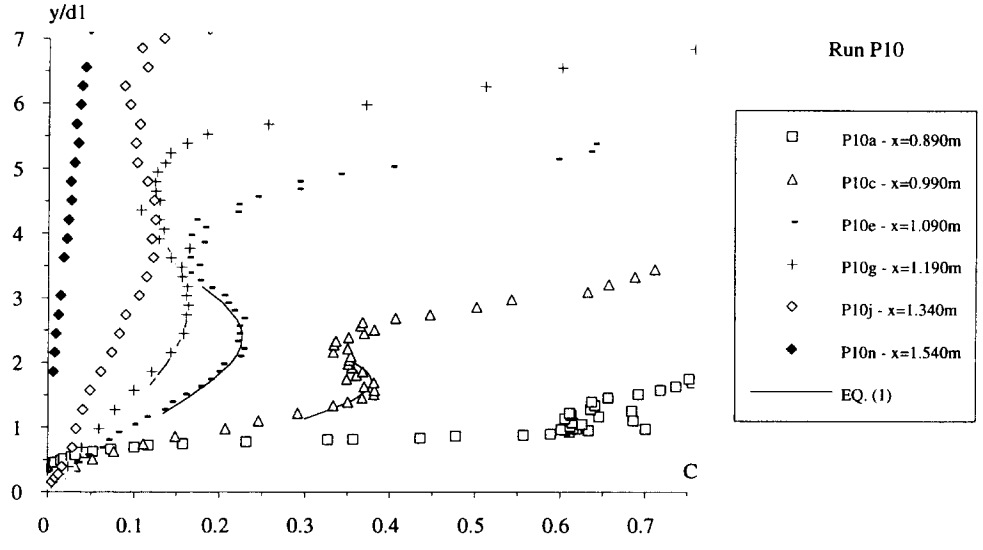

(B) Run C2, x_1 = 0.669 m, V_1 = 2.23 m/s, d_1 = 0.0158 m

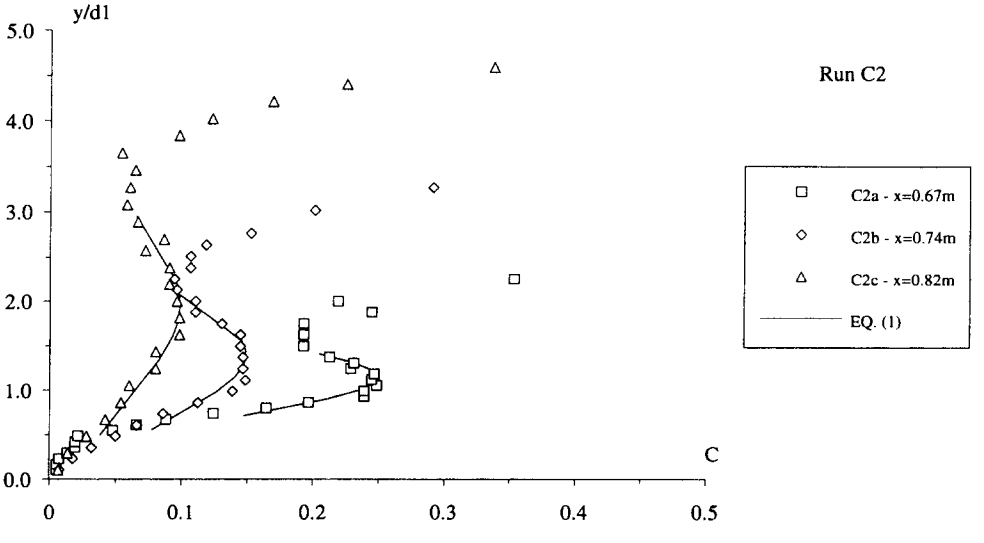

Figure 3. Air concentration distributions in a hydraulic jump with partially developed inflow conditions.

Figure 4. Photographs of turbulent shear layers. (A) Air bubble entrainment by a vertical supported jet (photo by the author), $x_1 = 0.12$ m, $V_1 = 4.3$ m/s, $d_1 = 0.011$ m (flow from the top to the bottom—note the vertical support on the left of the flow, the perspex window allowing to see the air bubble entrainment and the "white" downward diffusion cone. (B) Hydraulic jump with partially developed inflow conditions (photo by the author), $x_1 = 0.4$ m, $V_1 = 4.1$ m/s, $d_1 = 0.012$ m (flow from the right to the left—note the large air bubbles on the top left and the water droplet ejections downstream of the jump toe).

3.2. *Structure of the bubbly flow region*

The structure of the air–water flow in the turbulent shear layer was investigated using a high-speed camera. The main features of each experimental flow are summarized below.

3.2.1. Supported plunging jet. With the supported jet, the dispersion of entrained air bubbles forms two distinct regions: (1) a "diffusion cone" with a downward flow motion induced by the plunging liquid jet and (2) a swarm of rising bubbles which surrounds the former one.

In the diffusion cone (region 1), large quantities of air bubbles are entrained at high velocities [figures 2 and 4(A)]. The entrained bubbles are subjected to large shear stresses and broken up

(A) Vertical supported jet

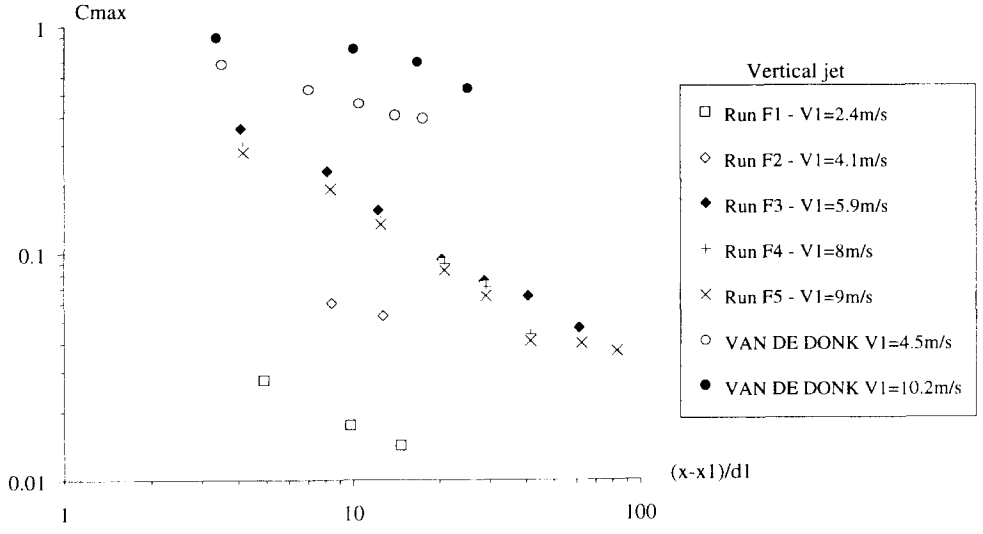

(B) Hydraulic jumps with partially developed inflow conditions

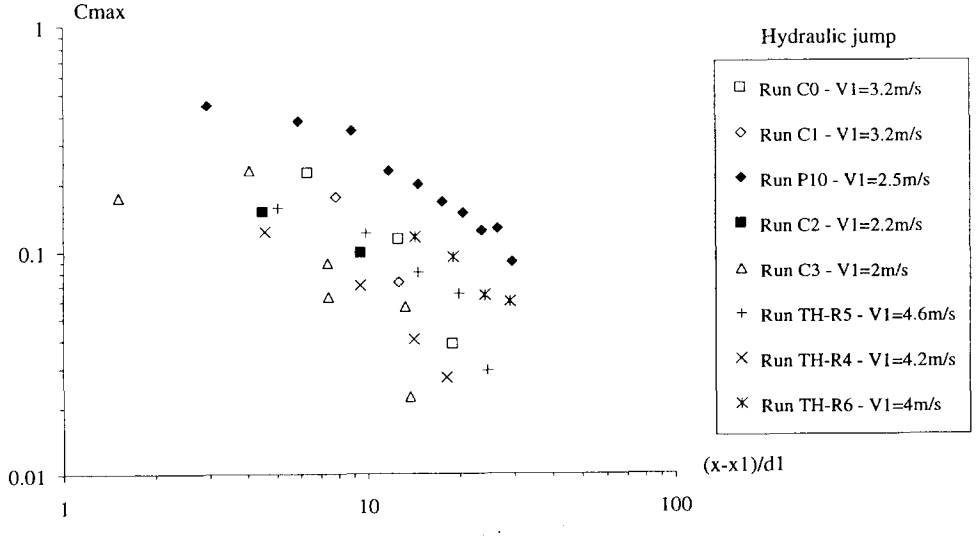

Figure 5. Longitudinal decay of the maximum air content C_{max}.

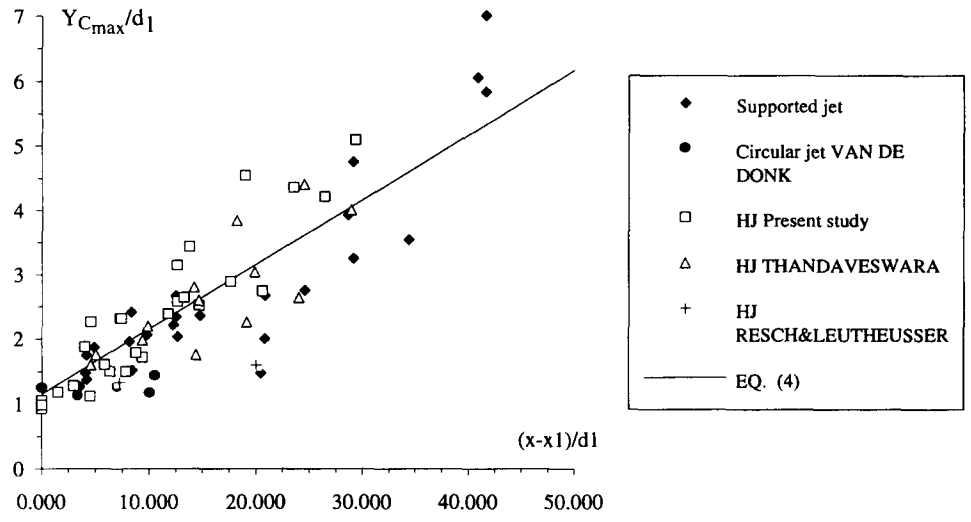

Figure 6. Location of the maximum air content $Y_{C_{max}}/d_1$ as a function of the dimensionless distance along the shear layer $(x - x_1)/d_1$.

into bubbles of smaller sizes. In a recent review, Bin (1993) highlighted the lack of information on the velocity profiles and on the momentum diffusion in two-dimensional air–water shear layers.

In the swarm of rising bubbles (region 2), the bubble motion is driven by buoyancy. Visual observations indicate that the air bubble motion is roughly vertical and that the bubble velocity nearly equals the bubble rise velocity in still water. For impact velocities V_1 larger than 2 m/s, it was observed that the lower edge of the diffusion cone (region 1) starts interfering with the flume bottom (located at $x = 1.8$ m).

3.2.2. Hydraulic jump. High-speed photographs and air concentration measurements enabled a comprehensive description of the bubbly flow region of a hydraulic jump. The following summarizes the findings of the present study and the earlier investigations by Thandaveswara (1974), Resch *et al.* (1972, 1974) and Babb & Aus (1981).

The air–water flow of a hydraulic jump includes three regions: (1) a turbulent shear layer with smaller air bubble sizes and high air content, (2) a "boiling" flow region characterized by the

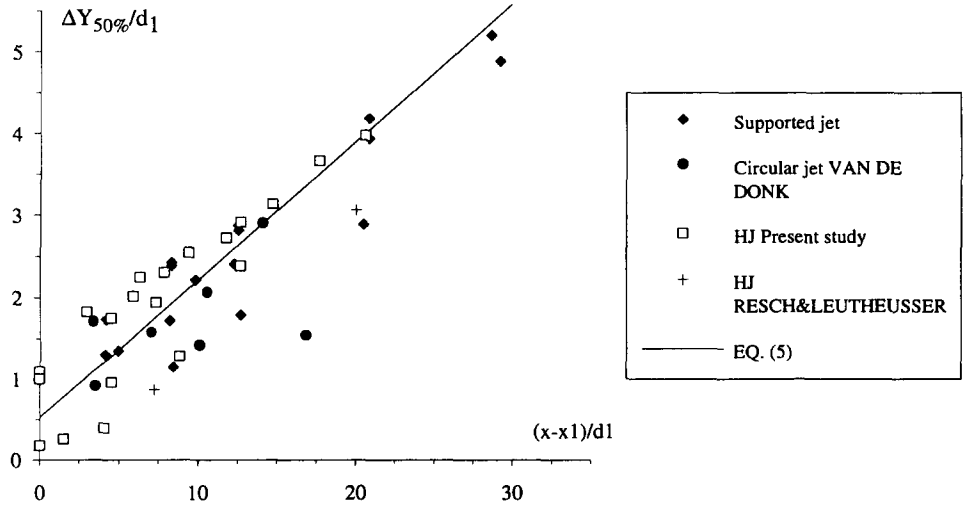

Figure 7. 50%-band width $\Delta Y_{50\%}/d_1$ versus the distance along the shear layer $(x - x_1)/d_1$.

Table 2. Location of the maximum velocity gradient in turbulent shear layers

Ref. (1)	y_{50}/d_1 (2)	Comments (3)
Vertical jets		
Chanson & Cummings (1994a)	$1 + (0.024*V_1 + 0.226)*\frac{x - x_1}{d_1}$	Supported jet. V_1 in m/s
Hydraulic jumps		
Rajaratnam (1965)	$0.5 + 0.065*\frac{x - x_1}{d_1}$	Re-analysis of several plane wall jet experiments
	$1 + 0.0805*\frac{x - x_1}{d_1}$ (†)	Hydraulic jump experiments
Ohtu *et al.* (1990)	$\frac{0.330}{\sqrt{Fr_1}}*\frac{x - x_1}{d_1}$	Partially developed inflow $(x - x_1)/d_1 < 34$
	$\frac{0.370}{\sqrt{Fr_1}}*\frac{x - x_1}{d_1}$	Fully-developed inflow $(x - x_1)/d_1 < 40$
Ohtu *et al.* (1990)	$1 + 0.0737*\frac{x - x_1}{d_1}$ (†)	Partially developed inflow $(x - x_1)/d_1 < 30$
	$1 + 0.1114*\frac{x - x_1}{d_1}$ (†)	Fully-developed inflow $(x - x_1)/d_1 < 40$
Related shear flows		
Albertson *et al.* (1948)	$1 + 0.033*\frac{x - x_1}{d_1}$ (†)	Monophase plane jets (air). Developing flow region
Rajaratnam (1976)	$1 + 0.041*\frac{x - x_1}{d_1}$	Monophase free jet (air). Data from Liepmann & Laufer (Liepmann & Laufer 1947), developing flows
Chanson (1993)	$1 + b*\frac{x - x_1}{d_1}$ with b =0.04 to 0.045	Plane high-velocity water jets discharging into the atmosphere. Free shear layer at the lower air–water interface

†Re-analysis by the author.
Fr_1 = upstream Froude number: $Fr_1 = V_1/\sqrt{g*d_1}$.

development of large-scale eddies and bubble coalescence and (3) a foam layer at the free-surface with large air polyhedra structures [figure 1(B)].

Air entrainment occurs in the form of air bubbles and air pockets entrapped at the impingement of the upstream jet flow with the roller. The air pockets are broken up into very thin air bubbles as they are entrained in the turbulent shear region, characterized by large air content as recorded by the air concentration probe (figure 3) and observed through the sidewall [figure 4(B)]. When the bubbles are diffused into regions of lower shear stresses, the coalescence of bubbles yields to larger bubble sizes and these bubbles are driven by buoyancy to the boiling region. Near the free-surface, the liquid is reduced to thin films separating the air bubbles. Their shape becomes pentagonal to decahedron as pictured superbly by Thandaveswara (1974).

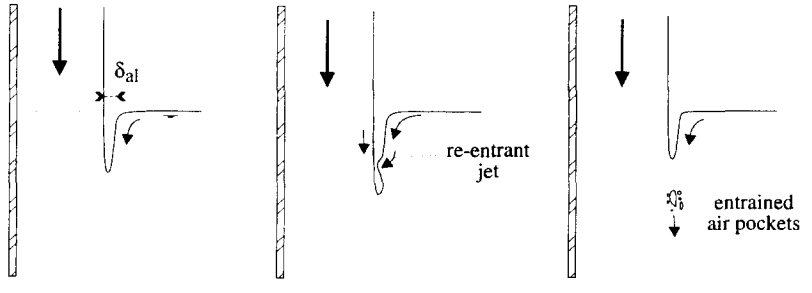

Sequence of large air pocket entrainment

Figure 8. Mechanisms of air entrapment by re-entrant jet.

4. CHARACTERISTICS OF THE TURBULENT SHEAR LAYERS

4.1. Air concentration distribution

For both series of experiments, the air concentration distributions in the turbulent shear layer exhibit the same shape, characterized by a highly aerated core (figures 2 and 3). The analysis of the experimental data (table 1) shows that the air concentration distributions in the turbulent shear region follow a Gaussian distribution:

$$C = C_{max} * \exp\left(- K * \left(\frac{y - Y_{C_{max}}}{\Delta Y_{50\%}} \right)^2 \right) \quad [1]$$

where C_{max} is the maximum air bubble concentration in the air diffusion layer, $Y_{C_{max}}$ is the location of the maximum air content, $\Delta Y_{50\%}$ is the 50%-band width (i.e. where $C = 0.5 * C_{max}$) and $K = 2.773$. Equation [1] is compared with the data in figures 2 and 3.

Further, the data indicate that the maximum air content decays exponentially in the flow direction (figure 5). For each flow situation, the longitudinal decay can be approximated by:

$$C_{max} \sim k' * \left(\frac{x - x_1}{d_1} \right)^{-0.59} \quad \text{(supported jet)} \quad [2]$$

$$C_{max} \sim k'' * \left(\frac{x - x_1}{d_1} \right)^{-0.54} \quad \text{(hydraulic jumps with partially developed inflow)} \quad [3]$$

where k' and k'' are constants, x is the distance along the channel, x_1 is the distance between the nozzle (or the gate) and the jet impact and d_1 is the initial flow depth (figure 1).

Interestingly, some properties of the air content Gaussian distributions are the same for the supported jet and hydraulic jump experiments. The 50%-band width and the location of the maximum air content, shown in figures 6 and 7, are best correlated by:

$$\frac{Y_{C_{max}}}{d_1} - 1 = 0.1002 * \frac{x - x_1}{d_1} + 0.1518 \quad \text{(hydraulic jump and supported jet)} \quad [4]$$

$$\frac{\Delta Y_{50\%}}{d_1} = 0.1689 * \frac{x - x_1}{d_1} + 0.5243 \quad [5]$$

Figures 6 and 7 (and [4] and [5]) suggest that the buoyancy has little effect upon the air content diffusion in a turbulent shear layer. A summary of all data is given in appendix A.

4.2. Interactions between the air diffusion layer and momentum shear layer

Some researchers recorded the velocity distributions in the shear layers of hydraulic jumps, at free shear layers, and in the developing flow region of jets (table 1). Their results indicated that the location of the maximum mean velocity gradient occurred at:

$$\frac{y_{50}}{d_1} = 1 + \beta * \frac{x - x_1}{d_1} \quad [6]$$

where y_{50} is the location where the mean velocity equals half of the maximum velocity, β equals 0.28–0.37 for the supported jet experiment (Chanson & Cummings 1994a) and varies typically between 0.073 and 0.081 for hydraulic jumps with partially developed inflows (table 2). For monophase jets, Rajaratnam (1976) estimated $\beta = 0.041$ from the data of Liepmann & Laufer (1947).

The above results imply that, for the hydraulic jump, the centreline of the air diffusion layer (i.e. $Y_{C_{max}}$) is located in the outward region of the momentum shear layer (i.e. $Y_{C_{max}} > y_{50}$), while the maximum air concentration is within the inward region of the shear layer for the supported jet (i.e. $Y_{C_{max}} < y_{50}$).

4.3. Discussion: air bubble entrainment by plunging jets

For the supported jet experiments, the data indicate an increase of the maximum air content with increasing mean inflow velocities V_1 from 2 to 6 m/s [figure 2(A) and (B)], but then a decrease of C_{max} when V_1 increases between 6 and 9 m/s [figure 2(B) and (C)]. This result was observed consistently through all the experiments and some runs were repeated for double-checking. The author believes that this "apparent" inconsistency reflects a change of air bubble entrainment mechanism.

Air bubble entrainment by plunging jet occurs for jet impact velocities larger than a critical value, usually called the inception velocity. For turbulent water jets, the inception velocity is about 0.9–1 m/s (Ervine *et al.* 1980; Chanson & Cummings 1994a). When $V_1 > 0.9$–1 m/s, air bubbles are entrained, and visual observations obtained during the investigations indicate two major air entrainment processes.

At low velocities (i.e. $V_1 < 2$–3 m/s), air bubble entrainment is caused by the pool water being unable to follow the undulations of the jet surface and small air pockets are formed. Air enters the flow following the passage of these disturbances through the interface between the jet and the receiving fluid. High-speed videocamera images indicate that most bubbles are entrained as pockets of bubbles and pockets of air, that are later broken up into smaller size bubbles as pictured by Chanson & Cummings (1994b). In slow motion, the air bubble entrainment appears a very unsteady pulsating process.

For larger jet impact velocities (i.e. $V_1 > 4$–8 m/s), experiments on both circular (Van De Sande & Smith 1973; Bonetto & Lahey 1993) and planar (present study) plunging jets indicate a qualitative change in the air entrainment process. A thin sheet of air, set into motion by shear forces at the surface of the jet, enters the flow at the impact point (figure 8). With the plane supported jet, visual observations indicate distinctively that the air sheet behaves as a ventilated cavity (e.g. Laali 1980; Michel 1984): the length of the air layer fluctuates considerably and air pockets are entrapped by a "re-entrant jet" mechanism (figure 8). The air pockets are entrained by discontinuous "gusts" at the lower end of the air layer. For jet velocities between 2 and 6 m/s, air sheet thickness δ_{al} of about 0.5–5 mm was observed with the jet experiment. The jet velocity at which the air layer appears is an inverse function of jet turbulence: i.e. for "smooth" jets, the air sheet will appear at larger velocities than for "rough" jets.

5. CONCLUSION

At the impact of a high velocity flow with a receiving body of water (pool or roller), a strong air bubble entrainment is observed. The "advection" of air bubbles within the turbulent shear layer is a complex function of the upstream flow conditions. With both a vertical supported jet and a hydraulic jump with partially developed inflow, the turbulent shear layer is characterized by a highly aerated core in which the air concentration follows a Gaussian distribution. The results indicate that the main properties of the Gaussian distributions are nearly "free" from buoyancy effects. Further, the air diffusion layer exhibits an exponential longitudinal decay.

With the vertical supported jet, a change of air entrainment mechanism is observed for impact velocities larger than 4–8 m/s. At larger inflow velocities, the air entrainment occurs via an air sheet set into motion by the impinging jet. The air layer behaves as a ventilated cavity, releasing intermittently large pockets of air that are later broken up into bubbles of smaller sizes.

Acknowledgements—The author acknowledges the assistance of Ms G. L. Qiao, Ms J. Patterson and Mr A. Feitz, and the discussions with Mr P. D. Cummings. He thanks also Dr B. S. Thandaveswara for providing his experimental data. The research project is supported by the Australian Research Council (Ref. A89331591).

REFERENCES

Albertson, M. L., Dai, Y. B., Jensen, R. A. & Rouse, H. 1948 Diffusion of submerged jets. *Trans. Am. Soc. civ. Engrs* **115,** 1571–1598.

Babb, A. F. & Aus, H. C. 1981 Measurements of air in flowing water. *J. Hydrol. Div., Am. Soc. civ. Engrs* **107,** 1615–1630.

Bin, A. K. 1993 Gas entrainment by plunging liquid jets. *Chem. Engng Sci.* **48,** 3585–3630.

Bonetto, F. & Lahey, R. T. Jr 1993 An experimental study on air carryunder due to a plunging liquid jet. *Int. J. Multiphase Flow* **19,** 281–294. See also Discussion **20,** 667–770.

Chanson, H. 1988 A study of air entrainment and aeration devices on a spillway model. Ph.D. thesis, Ref. 88-8, Department of Civil Engineering, University of Canterbury, New Zealand.

Chanson, H. 1993 Velocity measurements within high velocity air–water jets. *J. Hydraul. Res., IAHR* **31,** 365–382.

Chanson, H. 1995 Air bubble entrainment in free-surface turbulent flows. Experimental investigations. Report CH46/95, Department of Civil Engineering, University of Queensland, Australia.

Chanson, H. & Cummings, P. D. 1994a Modelling air bubble entrainment by plunging breakers. *Proc. Int. Symp. Wave Modelling*, IAHR, Vancouver, Canada.

Chanson, H. & Cummings, P. D. 1994b An experimental study on air carryunder due to plunging liquid jet—discussion. *Int. J. Multiphase Flow* **20,** 667–770.

Chanson, H. & Qiao, G. L. 1994 Air bubble entrainment and gas transfer at hydraulic jumps. Research Report No. CE149, Department of Civil Engineering, University of Queensland, Australia.

Ervine, D. A., McKeogh, E. J. & Elsawy, E. M. 1980 Effect of turbulence intensity on the rate of air entrainment by plunging water jets. *Proc. Inst. civ. Engrs*, Part 2, June, pp. 425–445.

Laali, A. R. 1980 Ecoulements ventilés. Etude de l'entrainement d'air. Cas d'une cavité formée entre un jet plan et une paroi solide. (Ventilated flows, study of air entrainment. Case of a cavity between a plane jet and a solid boundary.) Ph.D. thesis, University of Grenoble 1-INPG, Grenoble, France (in French).

Liepmann, H. W. & Laufer, J. 1947 Investigation of free turbulent mixing. NACA Tech. Note, No. 1257.

Michel, J. M. 1984 Some features of water flows with ventilated cavities. *J. Fluids Engng, Trans. ASME* **106,** 319.

Ohtu, I., Yasuda, Y. & Awazu, S. 1990 Free and submerged hydraulic jumps in rectangular channels. Report of the Research Institute of Science and Technology, No. 35, Nihon University, Japan.

Rajaratnam, N. 1965 The hydraulic jump as a wall jet. *J. Hydrol. Div., Am. Soc. civ. Engrs* **91,** 107–132. See also Discussion **92,** 110–123 and **93,** 74–76.

Rajaratnam, N. 1976 Turbulent jets. In *Development in Water Science*, Vol. 5. Elsevier, New York.

Resch, F. J. & Leutheusser, H. J. 1972 Le ressaut hydraulique: mesure de turbulence dans la région diphasique. (The hydraulic jump: turbulence measurements in the two-phase flow region.) *J. Houille Blanche* **4,** 279–293 (in French).

Resch, F. J., Leutheusser, H. J. & Alemu, S. 1974 Bubbly two-phase flow in hydraulic jump. *J. Hydrol. Div., Am. Soc. civ. Enrgs* **100,** 137–149.

Thandaveswara, B. S. 1974 Self aerated flow characteristics in developing zones and in hydraulic jumps. Ph.D. thesis, Department of Civil Engineering, Indian Institute of Science, Bangalore, India.

Van De Donk, J. 1981 Water aeration with plunging jets. Ph.D. thesis, Delft, The Netherlands.

Van De Sande, E. & Smith, J. M. 1973 Surface entrainment of air by high velocity water jets. *Chem. Engng Sci.* **28,** 1161–1168.

Von Mises, R. 1917 Berechnung von Ausfluss und Uberfallzahlen. *Z. ver. Deuts. Ing.* **61,** 447 (in German).

Wood, I. R. 1991 Air entrainment in free-surface flows. *IAHR Hydraulic Structures Design Manual No. 4, Hydraulic Design Considerations*. Balkema, Rotterdam, The Netherlands.

APPENDIX overleaf

APPENDIX A

Summary of the Experimental Results

Ref. (1)	Run (2)	$(x - x_1)/d_1$ (3)	C_{max} (4)	$(Y_{C_{max}}/d_1) - 1$ (5)	$\Delta Y_{50\%}/d_1$† (6)
Hydraulic jump					
Run C0	C0a	0.00	0.470	−0.01	
	C0b	6.33	0.223	0.50	2.24
	C0c	12.66	0.112	1.57	2.91
	C0d	18.99	0.038	3.53	
Run C1	C1f	0.00	0.317	−0.07	1.09
	C1g	7.85	0.173	0.50	2.30
	C1h	12.66	0.072	2.14	2.38
Run C2	C2a	0.00	0.249	0.05	0.99
	C2b	4.49	0.149	0.12	1.74
	C2c	9.43	0.098	0.72	2.54
Run C3	C3a	0.00	0.283	0.05	0.17
	C3b	4.05	0.229	0.88	0.39
	C3c	7.34	0.088	1.32	1.94
	C3d	13.29	0.056	1.63	
	C3e	1.52	0.173	0.18	0.25
	C3f	4.56	0.123	1.26	0.95
	C3g	7.41	0.062	1.32	
	C3h	13.80	0.022	2.43	
Run P10	P10a	0.00	0.624	−0.02	
	P10b	2.94	0.446	0.28	1.82
	P10c	5.88	0.378	0.60	2.01
	P10d	8.82	0.341	0.79	1.28
	P10e	11.76	0.227	1.39	2.72
	P10f	14.71	0.197	1.52	3.13
	P10g	17.65	0.164	1.89	3.66
	P10h	20.59	0.147	1.74	3.97
	P10i	23.53	0.123	3.36	
	P10j	26.47	0.125	3.21	
	P10k	29.41	0.089	4.09	
Thandaveswara (1974)	R6	14.38	0.115	0.76	
	R6	19.09	0.094	1.26	
	R6	23.99	0.063	1.64	
	R6	28.95	0.059	3.00	
Run R5	R5	5.03	0.155	0.76	
	R5	9.87	0.120	1.20	
	R5	14.65	0.080	1.60	
	R5	19.87	0.064	2.04	
	R5	24.52	0.029	3.40	
Run R4	R4	4.58	0.122	0.60	
	R4	9.41	0.070	0.98	
	R4	14.18	0.040	1.80	
	R4	18.16	0.027	2.84	
Resch & Leutheusser (1972)	F2.85-P2	7.25	0.164	0.34	0.87
	F6-P2	20	0.384	0.60	3.07
Supported jet					
Run F1	F1	4.92	0.027	1.06	1.35
	F1	9.83	0.017	2.37	2.21
	F1	14.75	0.014		
	F1	24.58	0.008		
	F1	34.42	0.009		
Run F2	F2	8.46	0.060	0.75	1.15
	F2	12.69	0.053	1.72	1.78
Run F3	F3	4.09	0.355	0.98	1.30
	F3	8.18	0.230	1.61	1.71
	F3	12.27	0.154	2.67	2.41
	F3	20.45	0.094	3.40	2.89
	F3	28.63	0.075	6.92	5.20
	F3	40.90	0.065	2.46	8.84
	F3	61.35	0.047		
Run F4	F4	4.17	0.294	1.63	1.72
	F4	8.33	0.188	2.63	2.38
	F4	12.50	0.139	3.28	2.81

†The half-value band width was estimated from the 85%-value band width.

APPENDIX A—continued

Ref. (1)	Run (2)	$(x - x_1)/d_1$ (3)	C_{max} (4)	$(Y_{C_{max}}/d_1) - 1$ (5)	$\Delta Y_{50\%}/d_1$† (6)
	F4	20.83	0.090	5.37	4.18
	F4	29.17	0.071	6.44	4.88
	F4	41.67	0.044		
	F4	62.50	0.040		
	F5	4.17	0.278	0.96	1.29
	F5	8.33	0.192	2.69	2.42
	F5	12.50	0.134	3.38	2.87
	F5	20.83	0.084	5.00	3.94
	F5	29.17	0.064		
	F5	41.67	0.041		
	F5	62.50	0.040		
	F5	83.33	0.037		
Circular jet‡		§		§	§
Van De Donk (1981)	Fig. 3.22	0.0	0.775	0.247	0.977
	Fig. 3.22	3.52	0.681	0.261	0.908
	Fig. 3.22	7.04	0.526	0.261	1.57
	Fig. 3.22	10.56	0.454	0.433	2.06
	Fig. 3.22	14.08	0.404	0.428	2.90
	Fig. 3.22	17.61	0.392		
	Fig. 3.23	3.37	0.891	0.126	1.70
	Fig. 3.23	10.10	0.794	0.165	1.42
	Fig. 3.23	16.83	0.694	0.120	1.53
	Fig. 3.23	25.24	0.530		

†The half-value band width was estimated from the 20%-value band width.
‡Study of the developing flow region of the jet only.
§For comparison between the supported jet and circular jet data we use: $d_1 = \phi_1/2$.